J Bionic Eng 17 (2020) 241–253
DOI: https://doi.org/10.1007/s42235-020-0019-2

Journal of Bionic Engineering
http://www.springer.com/journal/42235

Linear Acceleration of an Undulatory Robotic Fish with Dynamic Morphing Median Fin under the Instantaneous Self-propelled Condition

Wenguang Sun[1], Zemin Liu[1], Ziyu Ren[1], Gang Wang[1], Tao Yuan[2], Li Wen[1*]

1. *School of Mechanical Engineering and Automation*, *Beihang University*, *Beijing* 100191, *China*
2. *AECC Hunan Aviation Powerplant Research Institute*, *Zhuzhou* 412000, *China*

Abstract

Fish commonly execute rapid linear accelerations initiated during steady swimming, yet the function of the median fins during this process is less understood. We find that the erection/folding time (from the starting time of the linear acceleration (0 s) to the starting time of the folding movement of the fin), as well as the spreading area of the median fins, actively change during the linear acceleration of the live largemouth bass (*Micropterus salmoides*). To better understand the influence of the folding time and the area change of the median fins on the linear acceleration, we implemented an undulatory biomimetic robotic fish with soft median fins that can be programmed to erect and fold, just like a live fish. To characterize the acceleration performance of the robotic fish, we developed a ‘‘self-propelled’’ experiment technique based on the Kalman filter and Proportional-Integral-Derivative (PID) control algorithm. The experiments on the robotic fish show the acceleration induced by fully-erected median fins increases by 46.3%. Fully-erected median fins positively contribute to propulsion primarily at the onset stage of the linear acceleration while result in a significant decrease in steady swimming speed by 25%, which suggests a large drag force is induced at the steady swimming stage due to the enlarged wetted area. Parametric sweeping experiments on erection/folding time and spreading area demonstrate a proper combination of the erection/folding time and the spreading area enhances the mean linear acceleration by up to 85%. Particle Image Velocimetry (PIV) results reveal that the vortexes shed by the erected dorsal fin are stronger than those shed by the folded fin. As the acceleration process progresses, the thrust generated by the dorsal fins gradually is weakened until only resistance is generated in the end. Our findings may shed light on the realization of controllable surfaces on high performance fish-inspired robotic systems in the future.

Keywords: robotic fish, linear acceleration, median fin, instantaneous self-propelled system

1 Introduction

In nature, fish can linearly accelerate from rest to a high speed with a maximum acceleration up to 32 $m \cdot s^{-2}$[1]. Previous studies on fish linear acceleration mainly focus on exploring the influence of the body kinematics and the body morphology on acceleration performance[2–5]. Both anguilliform swimmers, such as eels[2], and carangiform swimmers, such as bluegill sunfish[4], increase the beating amplitude and frequency during the linear acceleration. This kind of body movement may generate more thrust needed for linear acceleration, by generating a larger vortices ring[3], modulating the geometry of the vortex ring more axisymmetric[4] or reorienting jets of the vortex ring to be a more axial direction[2,4]. These features result in an efficient transfer of force into the wake[4].

Fish median fins, which can be actively controlled[6–12], play an important role in propulsion[13–15], stability[16], and maneuverability[17]. However, most of these studies are conducted when the fish are at rest or at the steady swimming state. Our previous study has revealed that the fish median fin does have a significant influence on the linear acceleration performance[5]. While, the dynamic morphing of the median fins, which is reported in our current study (Fig. 1), is still less understood. In particular, the influence of the erection/folding time (from the starting time of the linear acceleration (0 s) to the starting time of the folding movement of the fin) of the median fins on linear acceleration remains unexplored.

Fish-inspired robotic models have been used to explore the mechanisms of pectoral fin motion[18], caudal fin motion[19] and undulatory fish body mo-

***Corresponding author:** Li Wen
E-mail: liwen@buaa.edu.cn

tion[20–22]. In order to investigate the influence of the dynamic morphing median fins on a swimming fish, we developed a robotic fish model that has an undulatory body and multiple foldable median fins based on our previous work[5]. Apart from the robot, it is also essential to set up a self-propelled system that excludes the effects of the tethered force. Wen *et al*. presented a self-propelled method based on a PID controller[5], but the achieved self-propelled speed is constant, which deviates from the fact that the instantaneous velocity of a fish fluctuates with time even at the steady swimming state[23–25]. The linear acceleration, which result in a time-varying speed, cannot be studied *via* the previous experimental approach.

In this study, we first confirmed the median fin movement during linear acceleration in real animals. Then a self-propelled experimental technique based on a force-feedback method was proposed to satisfy the self-propelled experimental condition. Lastly, this technique was applied to a robotic fish model to investigate how the dynamic morphing median fins (the timing and the area of fin erection/folding) affect the linear acceleration performance of the robotic fish.

2 Materials and methods

2.1 Fin motions of largemouth bass during linear acceleration

Largemouth bass (*Micropterus salmoides*) were housed in a separate 40 liter aquarium in the laboratory, and kept under a 12 h : 12 h light : dark photoperiod. Water temperature was kept constant about 20 ˚C (± 1˚C). Three basses (mean Body Length (*BL*) of 15 cm) that range from 14.7 cm to 15.4 cm were studied with five individual tests. Each bass was trained to swim in a variable-speed freshwater flow tank with a 25 cm wide, 25 cm deep, and 80 cm long working section. Before the experiment, the bass was delivered into the flow tank and then swam at two preset flow speeds (1 $BL{\cdot}s^{-1}$ and 2 $BL{\cdot}s^{-1}$). During the procedure, the bass was gently maneuvered into position in front of the cameras by using a wooden probe. After a period of steady swimming in the flow, the bass periodically accelerated linearly in response to a stimulus (produced by a wooden stick) behind them. The median fin area (S_c) and the linear acceleration were filmed as the fish began from steady locomotion at these two flow speeds (1 $BL{\cdot}s^{-1}$ and 2 $BL{\cdot}s^{-1}$) with synchronized ventral and lateral high-speed cameras (Photron PCI-1024, 1-megapixel resolution) at 1000 fps.

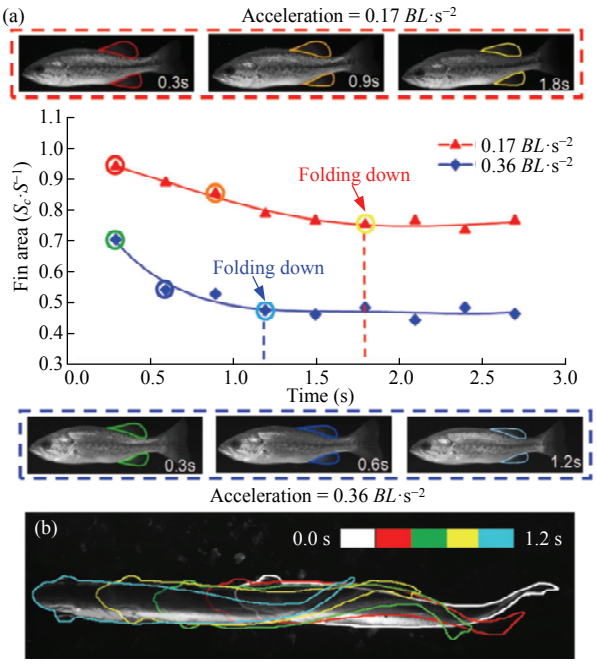

Fig. 1 Median fin movement in live fish acceleration. (a) Movements of the soft-rayed dorsal/anal fins of the same bass fish (*Micropterus salmoides*) during different linear acceleration (a = 0.17 $BL{\cdot}s^{-2}$ and 0.36 $BL{\cdot}s^{-2}$). Different colors indicate changes of fin area. All images were selected when the median fin moved at the same time during each beating cycle. (b) Composite image of the same bass fish during linear acceleration. The body profiles were extracted with a time interval of 0.24 s. Frames from t = 0 s to t = 1.2 s show a series of tail beats of four cycles during linear acceleration..

2.2 Biomimetic robotic fish with soft median fins

A biomimetic robotic fish with multiple median fins (including a spiny dorsal fin, a soft dorsal fin, an anal fin and a caudal fin) was developed in our study (Fig. 2). All biomimetic median fins were designed based on the morphology of largemouth bass (*Micropterus salmoides*). To mimic the folding/erecting movement of the dorsal/anal fins, four fin rays were designed to rotate around the shaft on the base through the cable-driven mechanism (Fig. 2a). The Kevlar fiber (0.5 mm in diameter) connected four fin rays in series and linked with a soft actuator mounted on the bottom of dorsal/anal fins. When the soft actuator was pressurized, transmitted by the cable-driven mechanism, the soft

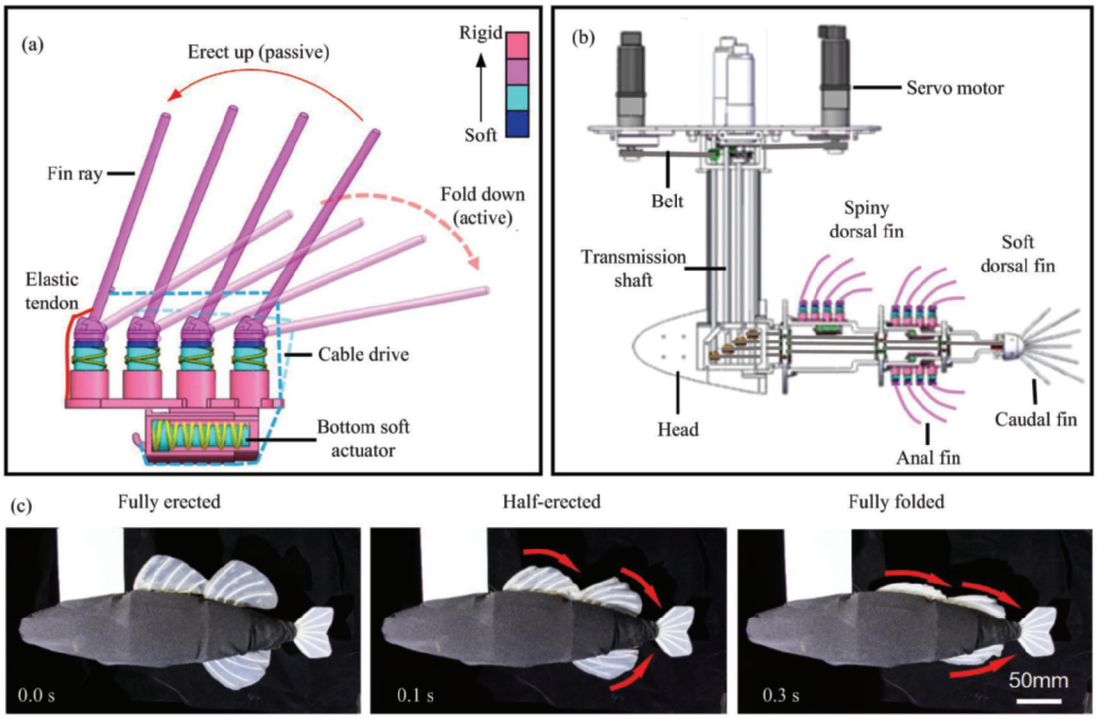

Fig. 2 The biomimetic robotic fish with median fin. (a)The side view of dorsal/anal fin model. The erect/fold motions are accomplished by the cable which translates the linear movement of the bottom soft actuator into the rotational movement of the fin. The color bar shows the stiffness of materials. (b) The biomimetic robotic fish with biomimetic spiny dorsal fin, soft dorsal fin, anal fins and caudal fin. All fins positioned relatively proportional to the BL of the real fish. Robotic fish has four moving segments which are driven by four Servo motors with encoder. Each motor provides a Degree of Freedom (DOF) to the robotic fish, and gets real-time position value from the encoder. (c) Movements of the dorsal/anal fins of the biomimetic robot fish during linear acceleration. The area of the spiny dorsal, soft dorsal/anal fins together (in lateral view) is *S*, 0.6 *S*, and 0.2 *S* for fully-erected, half-erected, and fully folded conditions, respectively (*S* is the total area of median fins). The red arrows indicate the direction of the folding soft fins. Scale bar is 50 mm.

actuator's linear motion can result in the folding motion of median fins. Additionally, an elastic tendon was fixed between the first fin ray and the base to generate a preload force of about 0.8 N, which maintained the erection of median fins when the soft actuator was inactive. Fin rays and skeleton structures were fabricated by using multi-material 3D printing technology. The fin rays were covered by fin membranes made of silicone material.

The dorsal and anal fins can be accurately controlled to fold from $S_c = S$ to $S_c = 0.2\ S$ by programming the pressure of actuator from 0 KPa to 250 KPa with the pneumatic system (Fig. 2c). Compared with the robot described in Wen *et al*.[5], we improved the four-bar linkage mechanism to a cable driven mechanism that enable the dorsal/anal fins folding down at a fast speed (26% faster). The minimum of folded area of dorsal/anal fins decreases by 10% with the cable driven mechanism.

The body of the biomimetic robotic fish consists of five sections, a fixed head segment and four moving segments (Fig. 2b). The body of the biomimetic robot fish has a total BL of 58.8 cm and mass of 2.79 kg. More details on the biomimetic robotic fish refer to our previous articles[5]. In this study, we programmed the robotic fish to generate a carangiform like locomotion at a frequency of 1.0 Hz in 0.96 *BL* wavelength.

2.3 The instantaneous self-propelled control with a Kalman filter

In this study, we achieved the instantaneous self-propelled control with a Kalman filter. In our experimental apparatus, the biomimetic robotic fish was connected to the guide rail *via* a multi-component force transducer. From Newton's law of momentum, equations for the fish in the forward axial direction will satisfy:

$$F_{\mathrm{T}} + F_{\mathrm{D}} + F_{\mathrm{S}} = M_{\mathrm{f}} \frac{\mathrm{d}U}{\mathrm{d}t}, \tag{1}$$

where F_S denotes the instantaneous force generated by the guide rail in the forward direction, U represents the robotic fish's self-propelled swimming speed in the forward direction and M_f represents the mass of the robotic fish. When the biomimetic robotic fish swims freely underwater, there are two kinds of force: thrust force F_T produced by the tail waving; drag force F_D produced by water. So the condition for achieving self-propelled swimming is that the force F_S is always 0. Acquired by force sensor, F_S will be fed back to the self-propelled control algorithm, then the towing system will generate corresponding towing speed to make the F_S maintain 0.

The oscillation of the mechanical system was unavoidable and unpredictable, which was detrimental to force acquisition and strongly affected the stability of the control system. Therefore, we optimized the self-propelled method with a Kalman filter to preprocess the force signal before sending it back to the PID controller. In the linear acceleration period, we analyzed the dynamics of the guide rail system with the Kalman filter algorithm. Firstly, the linear system model of the guide rail in the linear acceleration stage was established as:

$$F_{S(k)} = F_{S(k-1)} + W_{(k-1)}, \tag{2}$$

$$z_{(k)} = F_{S(k)} + V_{(k)}, \tag{3}$$

where $F_{S(k)}$ is the estimated value of the axial force generated by the guide rail at time k, $z_{(k)}$ is the measured value of the axial force generated by the guide rail. $W_{(k-1)}$ and $V_{(k)}$ represent process noise and measurement noise of multi-component force transducer respectively. The core content of Kalman filter algorithm is to reconstruct the state vector (*i.e.* the axial force F_S) of the system by calculating the estimated value of the current moment with the estimated value (*i.e.* the axial force $F_{S(k)}$) of the previous moment and the observed value (*i.e.* the force $z_{(k)}$) of the current moment. The core content of Kalman filter algorithm is to reconstruct the state vector of the system by calculating the estimated value of the current moment with the estimated value of the previous moment and the observed value of the current moment. So the random interference was eliminated with the Kalman filter. The Kalman filter algorithm can be updated in two stages: time update and measurement update. The updating algorithm for each variable can be found in Table 1. The output of the Kalman filter, *i.e.*, the towing force F_S, was then sent to a PID controller. Finally, the towing force F_S will be transmitted to the motion coordinator (Trio MC206) for speed control. The detail algorithm of the instantaneous self-propelled method is list in Table 1. As described above, the robotic fish model fixed on a towing system can work under an instantaneous self-propelled condition.

2.4 The experimental apparatus and experimental method

Our experiment apparatus (Fig. 3a) can be divided into three parts, biomimetic robotic fish, instantaneous self-propelled guide rail, and DPIV system. The biomimetic robotic fish was connected to a multi-axis ATI Delta force transducer (Delta, ATI industrial, Inc.) which was fixed under the guide rail plate. The force transducer has a natural frequency of 3 kHz, high rigidity of 500 $N \cdot \mu m^{-1}$, and a sensitivity of 0.005 N in the axial direction. The force data produced by the robotic fish were collected with a DAQ card (PCI-6284, National Instrument Inc, USA) and transferred to PC. The robotic fish moved in a water tank that was 7.8 m × 1.2 m × 1.1 m and was in a mid-depth position of the tank to avoid the influence of the boundaries on all sides. The robotic fish was hung under a plate that has been mounted on the guide rail. The guide rail plate was driven by a 4000-watt AC motor (position accuracy 0.1 m, maximum speed 3 $m \cdot s^{-1}$) which allows the plate to follow the movement of the robotic fish.

Digital Particle Image Velocimetry (DPIV) system mounted on the carriage was used to record the flow field of the dorsal fin of the robotic fish. Neutrally-buoyant glass particles (20 μm diameter) were placed evenly into the water tank. The light sheet projected by a 5 W laser (532 nm wavelength, MGL-N-532, Changchun Xinchanye Inc., Changchun, China) was reflected by two mirrors at the middle line of dorsal fin (Fig. 3a). A horizontal particle plane (Fig. 3b) was illuminated by the laser light. The high-speed camera (SP5000, JAI Inc., Denmark) was mounted vertically on the carriage above the position of the dorsal fin (Fig. 3a). The particle movements were recorded in the horizontal plane at 250 frames per second. More details of the flow field process can refer to our previous work[20].

Table 1 The algorithm of instantaneous self-propelled method

Algorithm. The instantaneous self-propelled swimming with the Kalman filter	
	Input: the axial force F_S produced by the guide rail in the x direction
	Output: The rail drag platform follows the linear accelerated swimming of the biomimetic robot fish and reaches the steady swimming speed.
1	While (1) do
2	Read the PID parameter $K_p = 1.7$, $K_i = 0.1$, $K_d = 0.03$.
3	KalmanForce (F_S);
4	For $i = 1, \ldots, 50$ do
5	Calculate the sum $\boldsymbol{T} \leftarrow \sum_{i=1}^{50} F_S$
6	End for
7	The differential force $F_S(T) \leftarrow T/50$ was conducted by the Kalman filter.
8	PID processed force $\boldsymbol{F} \leftarrow K_p F_S(T) + K_i \sum \Delta F_S(T) + K_d[\Delta F_S(T) - \Delta F_S(T-1)]$.
9	The instantaneous self-propelled acceleration $\boldsymbol{a} \leftarrow F/M$ (total mass of the biomimetic robot fish $M = 20$ kg)
10	The instantaneous self-propelled velocity $\boldsymbol{v}_t \leftarrow \boldsymbol{v}_{t-\Delta t} + \boldsymbol{a} \cdot \Delta t$ (sampling interval $\Delta t = 50$ ms)
11	End while
12	Function KalmanForce (F_S)
13	Read the covariance of process excitation noise Q.
14	Read the covariance of measure noise R.
15	Read the Estimated covariance P.
16	At time k Estimate the value of the state variable $\hat{F}_{S(k)} \leftarrow \hat{F}_{S(k-1)}$.
17	The Estimated covariance $\hat{P}_{(k)} \leftarrow \hat{P}_{(k-1)} + Q$.
18	Kalman gain $K_{(k)} \leftarrow \hat{P}_{(k)} \times (\hat{P}_k + R)^{-1}$.
19	The filtered force $F_{S(k)} \leftarrow \hat{F}_{S(k)} + K_{(k)} \times (z_{(k)} - \hat{F}_{S(k)})$.
20	$P_k \leftarrow (1 - K_{(k)}) \times \hat{P}_{(k)}$
21	End function

According to the dorsal and anal fins' motion of the live fish during the linear acceleration, we conducted experiments with 44 combinations of relative median fin area (0.8 S, 0.6 S, 0.4 S, 0.2 S) and different folding time ($t_f = 0$ T, 1 T,…, 10 T, where T is the tail beat period of the robotic fish). Folding time is the time period between the robotic fish starting to swim (0 s) and the instant of triggering the median fin to fold down. For each area, the robotic fish model accelerated with fully-erected median fins from zero velocity and varied time that the median fins fold to the corresponding area. We recorded the speed profiles and the towing force (the positive direction is along the head of the robotic fish) until the robot fish reached a steady swimming state under the instantaneous self-propelled experiments. The self-propelled swimming acceleration (a) is calculated as the mean value of the ascent from the static state to the steady state velocity, *i.e*., the steady swimming velocity (U_{SPS}) over the acceleration time (t_a). Each force and speed profile is the mean from five repeated trials at each area and folding time ($N = 5$).

3 Results

3.1 Linear acceleration under instantaneous self-propelled swimming conditions

As the largemouth bass swims at a more substantial acceleration, dorsal and anal fins fold earlier to a smaller area (Fig. 1a). Fig. 1a shows that dorsal and anal fins fold down to $S_c = 0.8$ S at $t = 1.8$ s under accelerated swimming of 0.17 $BL \cdot s^{-2}$. When the largemouth bass swims at an acceleration of 0.38 $BL \cdot s^{-2}$, the dorsal and anal fins fold down to $S_c = 0.48$ S at $t = 1.2$ s.

We first measured the self-propelled swimming speed/acceleration using the traditional constant-speed towing method. The obtained result was then taken as the ground truth to validate the self-propelled technique proposed in this paper. For the constant-speed towing method, we drag the robotic fish with a series of constant

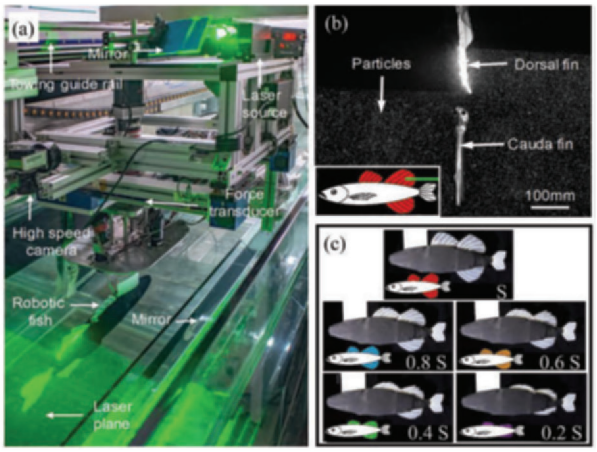

Fig. 3 The instantaneous self-propelled experimental apparatus for testing the biomimetic robotic fish. (a) Photograph of the schematic of the experimental device of the robotic fish. The primary components of the apparatus and the DPIV experiment settings are illustrated in the image. When the self-propelled system is operating, the robotic fish is swimming with velocity along the *x*-axis. (b) High-speed camera image of the illuminated particles in top view. The light green bar on the dorsal fin shows the position of the laser plane. (c) The robot fish with different median fin patterns (S_c = 0.2 *S*, 0.4 *S*, 0.6 *S*, 0.8 *S*, *S*). The movie of the robotic fish performing linear acceleration along the towing system is available in supplementary videos.

velocities or accelerations. The velocity/acceleration that results in a zero average towing force (F_S) is considered as the self-propelled swimming speed/acceleration. Using this method, the self-propelled swimming speed and acceleration measured for two cases are shown in Figs. 4a and 4b, respectively. The robot acquired a higher self-propelled swimming speed (U_{SPS} = 0.411 $BL{\cdot}s^{-1}$) and linear acceleration (a = 0.039 $BL{\cdot}s^{-2}$) when all fins were fully folded down than erected up (U_{SPS} = 0.39 $BL{\cdot}s^{-1}$, a = 0.037 $BL{\cdot}s^{-2}$).

Fig. 4c shows the instantaneous velocity profiles obtained through the self-propelled method. The self-propelled swimming speed can be read directly after the velocity profile becomes stable, which are 0.39 $BL{\cdot}s^{-1}$ for all fins erected up and 0.411 $BL{\cdot}s^{-1}$ for all fins folded down. The mean linear acceleration can be calculated through dividing the self-propelled swimming speed by the acceleration time. Unlike the instantaneous acceleration in the constant-speed towing method, the instantaneous acceleration of the robotic fish changed continuously with time in the self-propelled method.

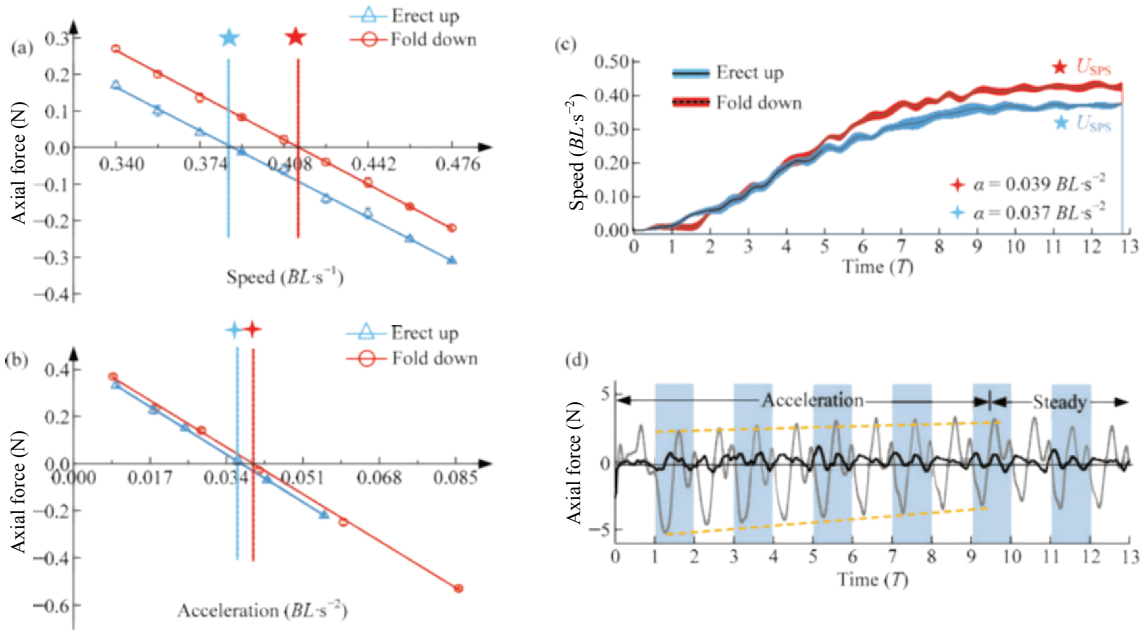

Fig. 4 The swimming performance of the robotic fish under towing method and self-propelled method. (a) The relationship between the towing force and the self-propelled swimming speed determined by the towing system. The star shows the steady speed (axial force equal to zero). (b) The relationship between axial force and acceleration, tring to determine the threshold acceleration for the towing system. The star shows the linear acceleration (the towing force equals to zero). (c) Different swimming speed performances between towing method and self-propulsion method. The solid line illustrates the towing method performance, and the dotted line illustrates the self-propulsion method performance. (d) Different axial force performances between towing method and self-propelled method. The black and gray lines indicate the towing force with the self-propelled method and the towing method, respectively. Error bars are ± 1 s.e.m. s.e.m. is standard error of the mean.

The instantaneous towing force F_S of the constant-speed towing method and the self-propelled method are compared in Fig. 4d. Although the time-averaged towing force obtained by the constant-speed towing method was zero over each flapping cycle during the steady swimming state, the towing force had a significant fluctuation with amplitude of 3 N. By using the self-propelled method, such fluctuation amplitude was greatly restrained to no more than ± 1 N. This further demonstrates that the self-propelled method can help to reduce the undesired force input from the guide rail.

3.2 Effect of the median fin area and folding time on linear acceleration

Both the folding time and area of the median fins are important factors that determine the self-propelled linear acceleration (Fig. 5). When the folding area of the median fin remained fixed, the self-propelled swimming acceleration increased and then decreased with the increase in folding time (Fig. 5a). The dotted line in Fig. 5a clearly shows the above change, which represents the distribution of the folding time when the maximum self-propelled linear acceleration is obtained in each folding area. When median fins of the robotic fish folded down to an area of S_c = 0.8 S at t = 4 T, the self-propelled swimming acceleration reached the maximum (a = 0.022 $BL{\cdot}s^{-2}$) which increased by 62.5%.

We found that even if the oscillation amplitude of the robotic fish changed from A = 0.05 BL to A = 0.1 BL, the law described above held true (Fig. 5b). Similarly, foe the median fin with the same folding area, the self-propelled linear acceleration increased and then decreased with the increase in the folding time. The dotted line shows the combination of the folding area and the folding time for maximum acceleration. However, the oscillation amplitude did cause the movement of the max point. When the median fins were folded to 0.6 S at t = 2 T, the maximum of the self-propelled linear acceleration (a = 0.044 $BL{\cdot}s^{-2}$) was obtained. The dynamic motion of the median fin can increase the linear acceleration of the biomimetic robot fish up to 85.7%.

Compared to the self-propelled linear acceleration, the steady swimming speed solely depends on the area of the median fins (Fig. 6). No matter the oscillation amplitude was 0.05 BL or 0.1 BL, the self-propelled swimming speed increased first and then decreased with the reduction of the folding area, and reached a maximum when the folding area was 0.6 S (Figs. 6a and 6b). The maximum self-propelled swimming speeds were U_{SPS} = 0.34 $BL{\cdot}s^{-1}$ and U_{SPS} = 0.44 $BL{\cdot}s^{-1}$ at the amplitude A = 0.05 BL and A = 0.1 BL (Figs. 6c and 6d). This is a significant increase of 18.5% and 21.7% respectively at the oscillation amplitude of A = 0.05 BL

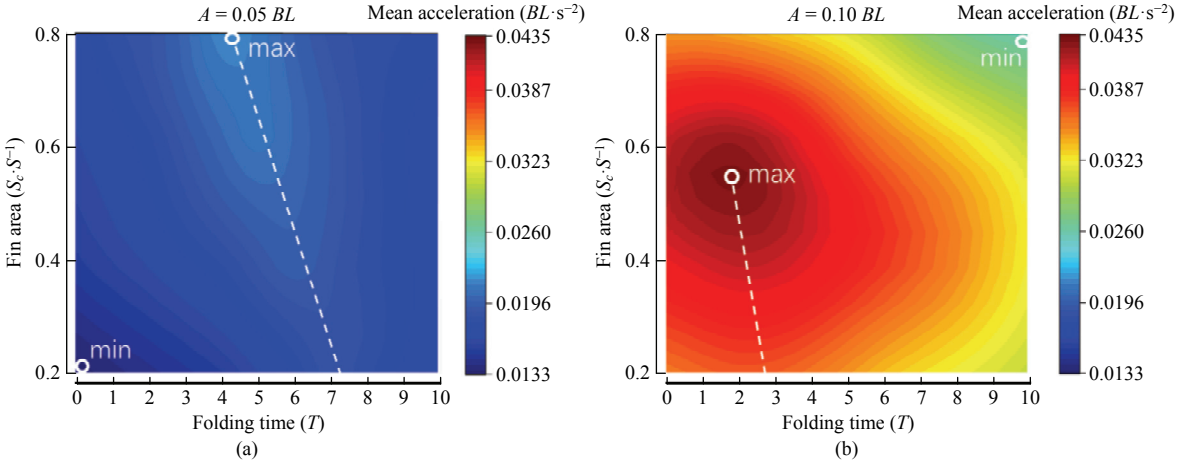

Fig. 5 The instantaneous self-propelled swimming performance of the biomimetic robot fish with different median fin patterns. The heat maps show the mean linear acceleration of robotic fish under self-propelled swimming at A = 0.05 BL (a) and A = 0.1 BL (b) (A is the oscillation amplitude of the caudal fin peduncle of the biomimetic robotic fish). x axial indicates the folding time that is the time it takes for the robotic fish to begin to swim until the middle fin begins to fold down. y axial indicates the fin area that robotic fish fins fold. The maximum acceleration and the minimum acceleration were marked out by the white circle in the heat map.

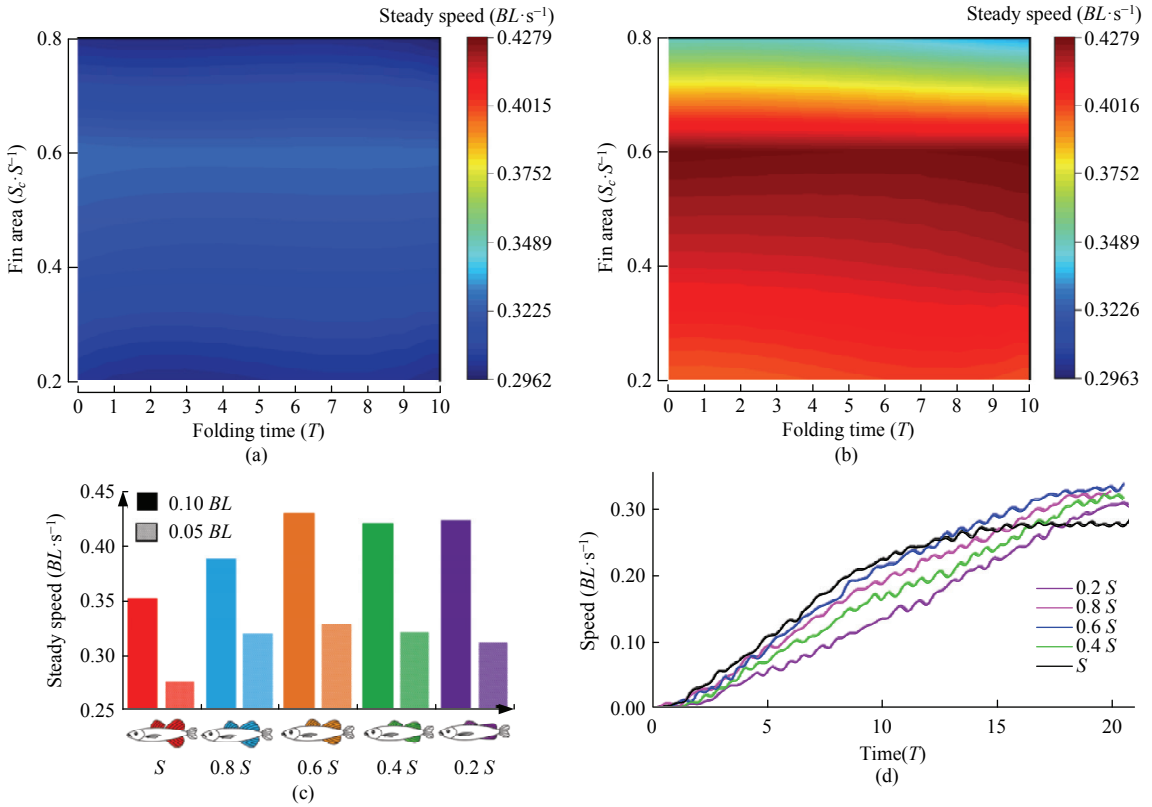

Fig. 6 The steady swimming speed of biomimetic robotic fish with different median fin states. The heat maps show the steady swimming speed of robotic fish under self-propelled swimming at $A = 0.05\ BL$ (a) and $A = 0.1\ BL$ (b). (c) The mean steady swimming speed with different fin area under self-propelled swimming condition. (d) The linear acceleration profiles of the biomimetic robot fish at 0.05 BL amplitude under self-propelled swimming condition.

and $A = 0.1\ BL$.

By analyzing the velocity profiles (Fig. 7a) of the robotic fish with different folding areas and the same folding time ($t_f = 2\ T$), we found that increasing the fin area can instantly increase the swimming speed in the initial stage of acceleration. However, the contribution of large area fins to self-propelled swimming is not obvious in the late stage of acceleration. Fig. 7a shows there is a steep rise in the speed of the self-propelled swimming (from $v = 0.068\ BL \cdot s^{-1}$ to $v = 0.238\ BL \cdot s^{-1}$) between $t = 2\ T$ to $t = 5\ T$ when the median fins fold down to $S_c = 0.8$ S. The different case is that the speed of the self-propelled swimming increases slowly (from $v = 0.068\ BL \cdot s^{-1}$ to $v = 0.170\ BL \cdot s^{-1}$) with the median fin of $S_c = 0.2\ S$. However, when the median fins fold from $S_c = S$ to $S_c = 0.6\ S$ at $t = 2\ T$, the biomimetic robot fish gets the maximum acceleration $a = 0.044\ BL \cdot s^{-2}$ and the largest steady swimming speed $v = 0.442\ BL \cdot s^{-1}$.

In the case of the same folding area of the median fins, the earlier the median fin folds, the more substantial linear acceleration of the biomimetic robotic fish would achieve (Fig. 7b). The biomimetic robotic fish obtained the maximum mean acceleration $a = 0.044\ BL \cdot s^{-2}$ when median fins folded down at $t = 2\ T$. However, the minimum acceleration was obtained ($a = 0.034\ BL \cdot s^{-2}$) when median fins folded down at $t = 9\ T$.

3.3 Wake flow of linear acceleration of robotic fish

Figs. 8a and 8b show the wake flow generated by the soft dorsal fin during the self-propelled linear accelerated swimming process. Wake flow patterns were investigated to explain the observed differences in acceleration with different folding time and median fin areas. We analyzed wake flows of the soft dorsal fin at $t = 1.5\ T$ and $t = 2.5\ T$ with median fin area $S_c = S$ (Fig. 8a) and $S_c = 0.6\ S$ (Fig. 8b).

Compared the flow filed shown in Figs. 8a and 8b, we found the fully erected dorsal fin ($S_c = S$) generated a larger vorticity ring and a smaller jet angle at $t = 1.5\ T$ than half-erected dorsal fin ($S_c = 0.6\ S$). The jet angle

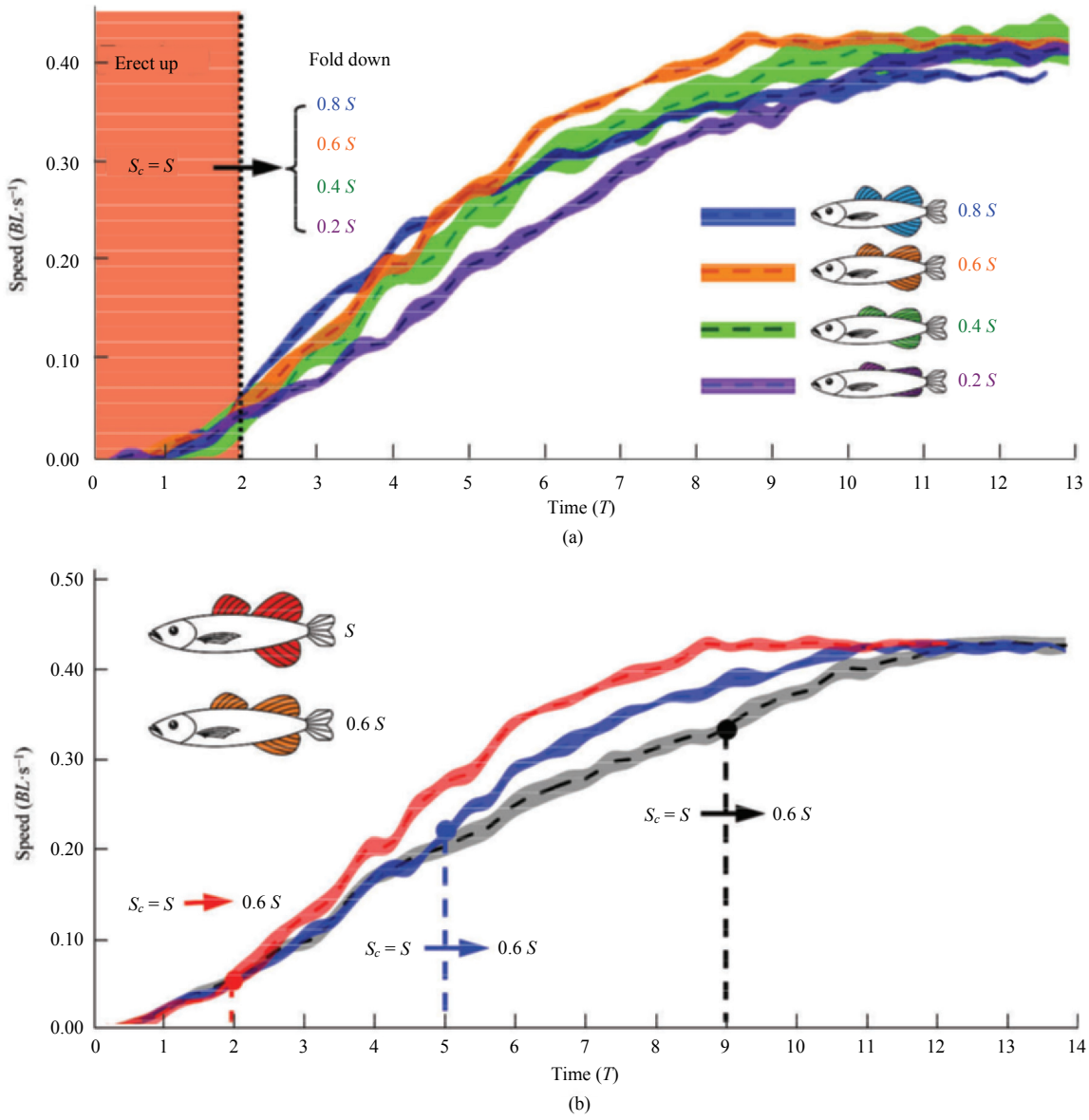

Fig. 7 The speed profiles of biomimetic robot fish under self-propelled swimming with different swimming patterns. (a) The self-propelled swimming speed profiles of biomimetic robot fish that dorsal/anal fins fold down from $S_c = S$ to different areas ($S_c = 0.8\ S$, 0.6 S, 0.4 S and 0.2 S) at $t = 2\ T$. The red shaded area indicates the times when the dorsal and anal fins are fully-erected. (b) The self-propelled swimming speed profiles of biomimetic robot fish at a different time ($t = 2\ T$, 5 T and 9 T) that dorsal/anal fins area change from $S_c = S$ to 0.6 S. Error bars are s.e.m.

(defined in Fig. 8) of the wake flow is $\theta = 43^\circ$ when all median fins were erected up at $t = 1.5\ T$ while $\theta = 50^\circ$ when all median fins were half folded (Fig. 8a). At $t = 2.5\ T$, the vorticity produced by the fully-erected fin ($S_c = S$) decreased significantly and the jet angle increased to $\theta = 60^\circ$. However, the vorticity and the jet angle produced by the half-erected fin ($S_c = 0.6\ S$) did not change much.

We analyzed the vortices generated by the dorsal fin through calculating the circulation and the jet angle during the linear acceleration under different fin areas (Figs. 8c and 8d). We found that the fully-erected dorsal fin ($S_c = S$) produced a stronger vortex pair, and the circulation of vortices gradually weaken over time (Fig. 8c). Compared with vortices generated by smaller dorsal fin area ($S_c = 0.6\ S$), the vortices generated by fully erected dorsal fin decayed notably faster. The jet angle increased from $\theta = 31^\circ$ to $\theta = 88^\circ$ after $t = 9\ T$ under the median fins fully-erected ($S_c = S$), and it increased from $\theta = 42^\circ$ to $\theta = 88^\circ$ after $t = 11\ T$ under the median fins folding to $S_c = 0.6\ S$ (Fig. 8d).

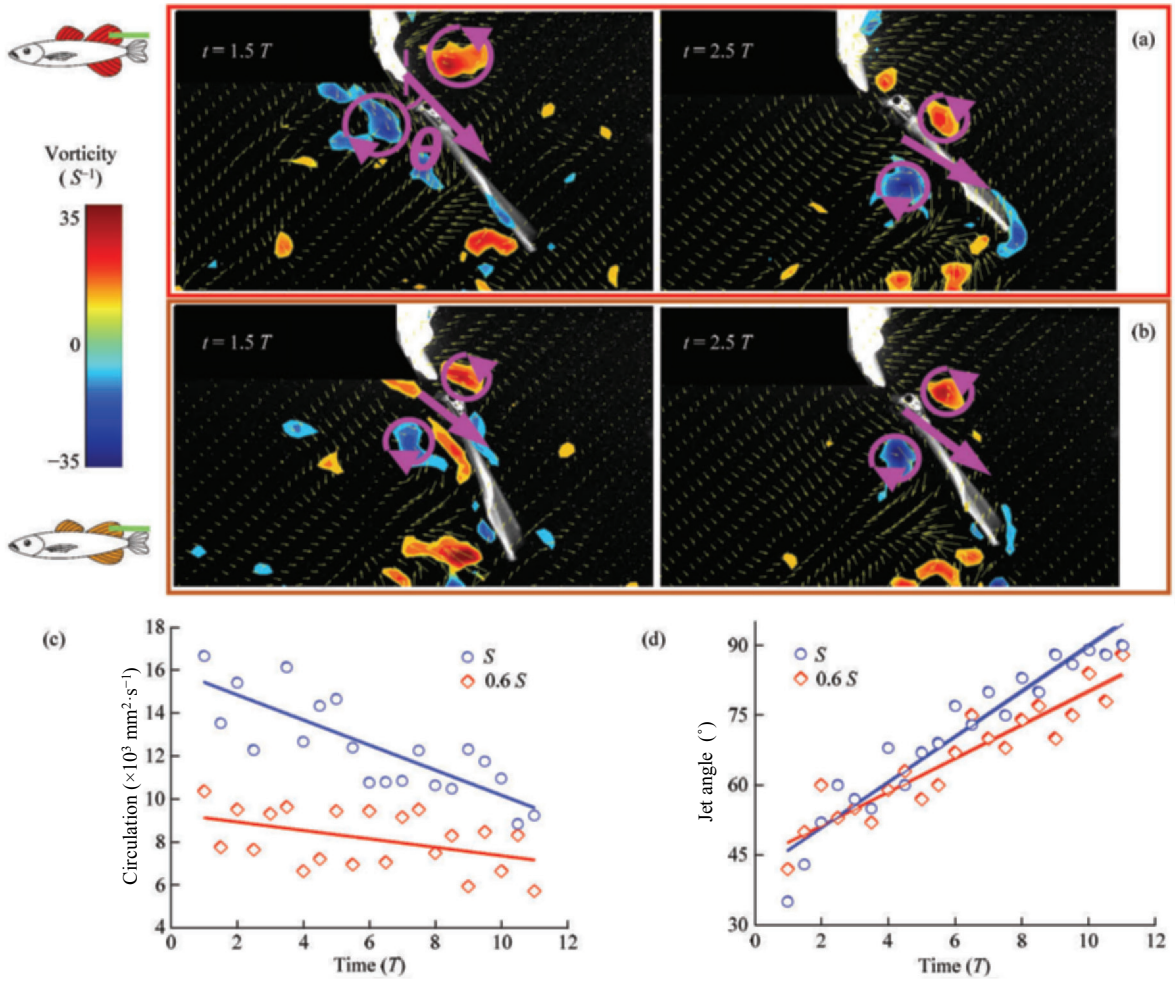

Fig. 8 Comparison of the wake of different median fin patterns during the linear acceleration at the same time instant (t = 1.5 T and 2.5 T). The wake flow of soft dorsal fin of the robotic fish when all fin is fully-erected (a) (S) and is half-erected (b) (0.6 S). The pink circle marks out the vortex generated by the soft dorsal fin. The pink arrows indicate the jet direction. θ indicates the angle between jet direction and motion direction. (c) The circulation of vortices versus time during linear acceleration swimming under different fin areas. (d) Jet angle of the wake flow versus time during linear acceleration swimming under different fin areas. The solid line indicates significant linear regression ($P < 0.001$).

4 Discussion

4.1 The self-propelled method with Kalman filter

During the linear acceleration, the acceleration rate and velocity of fish change dynamically throughout the process. For hydrodynamic experiments, it is essential to acquire the time-varying acceleration and velocity during the entire linear accelerated swimming. There are two main conventional approaches to quantify the hydrodynamic performance of the biomimetic robotic fish: the active towing method[5,26,27] and the passive towing method[28–30]. Measuring the steady swimming speed and the mean acceleration with the towing method has been validated in our previous work[5]. However, the constant towing speed and acceleration cannot reflect the time-varying velocity fluctuation during the swimming. Moreover, massive experimental data are required to determine the steady swimming speeds and mean acceleration[5]. For the passive towing method, the additional mass of the robotic fish model and the experimental apparatus affect swimming speed[29]. In this study, the feed-back control algorithm guarantees the self-propelled experimental condition is met in all trials (Fig. 4d). The steady swimming speed and the acceleration rate can be acquired from one single measurement (Fig. 4c). The force used to accelerate the added mass, such as the mass of the whole PIV setup (the mass of the PIV system is 17 kg), was totally provided by the servo motor driving the rail system rather than the robotic fish itself. Therefore, the influence of the added mass on

robotic fish acceleration was excluded from the measurement.

4.2 The effect of dynamic area change of the median fins on linear accelerated swimming

Our experiments demonstrate the importance of the dynamic area changing of the median fins on linear acceleration performance. The acceleration reaches its maximum value (0.044 $BL{\cdot}s^{-2}$) when the robotic fish fins were programmed to fold down to 0.6 S at $t = 2\ T$ (Fig. 5b). However, if the fins' areas remain the same during the whole swimming process, the acceleration is relatively insignificant compared with the dynamic area changing method (Fig. 5).

Meanwhile, our experimental results are also consistent with biological data. According to the studies of live fish, dorsal and anal fins are rapidly erected to increase their surface area at the fast start[31,32]. Except for the stabilizing function[10], a more important function of erected dorsal and anal fins is to generate thrust[33]. The experimental data of Tytell *et al*. suggests that the dorsal and anal fins contribute 37% of total momentum[32]. Fully-erected dorsal and anal fins are not always benefited for swimming performance, large wetted areas may contribute to maximizing thrust at the onset stage of the linear acceleration[34,35], but large areas can also make the fish subject to greater drag to fluid due to increased speed[17]. Therefore, as swimming speed increases, the drag of fully-erected dorsal and anal fins increases and exceeds the thrust generated by dorsal and anal fins. As a result, biological fishes choose to decrease the fin areas under high velocity for better swimming performance[5]. To verify this biological result, we conducted several experiments and the results (Fig. 7a) show that the biomimetic robotic fish with half-erected median fins obtain the maximum steady swimming speed, which is consistent with the biological hypothesis. Obviously, biological fin areas are not constant during the whole process, fishes would fold their fins to a smaller area at a specific moment during the acceleration. Therefore, the folding time, as well as the area of the median fin, play a significant role in the linear acceleration.

4.3 The wake flow behind the dorsal fin

At the start-up stage ($t = 1.5\ T$) of the linear acceleration, we found that the wake jet angles were $\theta = 43^\circ$ with the fully-erected dorsal fin, while the wake jet angles were $\theta = 50^\circ$ with the half-erected dorsal fin. For the fully-erected dorsal fin, the vorticity is stronger than that of the half-erected ones. Comparison of the wake flow between the "fully-erected" fins and the "half-erected" fins indicates that the axial thrust force caused by a larger median fin is stronger than the smaller fin, which coincides with the findings that the biomimetic robot fish with large fins have higher acceleration before $t = 2\ T$ (Fig. 7). From $t = 1.5\ T$ to $t = 2.5\ T$, the wake strength of the fully-erected dorsal fin decreased rapidly, and the jet angle increased from $\theta = 43^\circ$ to $\theta = 60^\circ$. However, the wake strength and the jet angle ($\theta = 53^\circ$) of the half-erected dorsal fin has little change during this time period. As swimming speed increases, so does the interaction force between fins and water, resulting in a large drag force for larger fin area under high swimming speed. Therefore, the larger area dorsal fin produces stronger axial thrust force at the starting stage, but weaker axial thrust at high swimming speed. Our finds in this paper further confirm the conclusions obtained by previous literature. Wen *et al*. found there are two ways to increase the axial force: the smaller jet angle and the stronger wake[5]. Moreover, during the onset stage, erected soft dorsal and anal fins contribute significantly to the onset[5].

Meanwhile, we found that the orientation and circulation of the dorsal fin wake differed substantially during the linear acceleration (Figs. 8c and 8d). Tytell *et al*. reported the wake flow of eels (*A*. *rostrata*) during linear acceleration and noted that the caudal momentum jets were oriented in a more downstream direction (*i.e*., produced smaller jet angle), with the addition of axial momentum relative to steady swimming wake flows[2]. Figs. 8c and 8d show that the dorsal fin's thrust contribution to propulsion decreases with time during the linear acceleration.

5 Conclusion

In this paper, we found that the folding time and median fin area are both essential for the linear acceleration performance apart form the body locomotion which has been shown in previous literatures. Our result shows that the maximum mean acceleration is acquired

in the way that dorsal and anal fin of biomimetic robotic fish moves from fully-erected state to half-erected state at $t = 2\ T$ regardless of the body amplitude. Fully-erected median fins produce the most significant axial thrust force at the initial starting stage of the linear acceleration, which generate large drag force at the steady swimming state. Therefore, it is crucial to find the optimal equilibrium between folding time and area for the linear acceleration. It should be noted that the current study did not take into account the folding speed of dorsal and anal fins yet. The folding speed may be another interesting factor that may affect the linear acceleration, and this will be explored in the future.

Acknowledgment

This work was supported by the National Science Foundation support projects, China (Grant Nos. 91848105, 61822303, 61633004 and 91848206), in part by National Key R&D Program of China (Grant Nos. 18YFB1304600 and 2019YFB1309600).

* All supplementary materials are available at https://doi.org/10.1007/s42235-020-0019-2.

References

[1] Tuna Lab @Large Pelagics. *Are Sailfish the World's Fastest Fish in the Ocean*? [2015-05-21], https://medium.com/@Tuna/is-sailfish-the-world-s-fastest-fish-in-the-ocean-68c2f7c82779

[2] Tytell E D. Kinematics and hydrodynamics of linear acceleration in eels, Anguilla rostrata. *Proceedings of the Royal Society of London*. *Series B*: *Biological Sciences*, 2004, **271**, 2535–2540.

[3] Wise T N, Schwalbe M A B, Tytell E D. Hydrodynamics of linear acceleration in bluegill sunfish, *Lepomis macrochirus*. *Journal of Experimental Biology*, 2018, **221**, 190892.

[4] Akanyeti O, Putney J, Yanagitsuru Y R, Lauder G V, Liao J C. Accelerating fishes increase propulsive efficiency by modulating vortex ring geometry. *Proceedings of the National Academy of Sciences*, 2017, **114**, 13828–13833.

[5] Wen L, Ren Z Y, Di Santo V, Hu K N, Yuan T, Wang T M, Lauder G V. Understanding fish linear acceleration using an undulatory biorobotic model with soft fluidic elastomer actuated morphing median fins. *Soft Robotics*, 2018, **5**, 375–388.

[6] Jayne B C, Lozada A F, Lauder G V. Function of the dorsal fin in bluegill sunfish: Motor patterns during four distinct locomotor behaviors. *Journal of Morphology*, 1996, **228**, 307–326.

[7] Lauder G V, Nauen J C, Drucker E G. Experimental hydrodynamics and evolution: Function of median fins in ray-finned fishes. *Integrative and Comparative Biology*, 2002, **42**, 1009–1017.

[8] Chadwell B A, Standen E M, Lauder G V, Ashley-Ross M A. Median fin function during the escape response of bluegill sunfish (*Lepomis macrochirus*). I: Fin-ray orientation and movement. *Journal of Experimental Biology*, 2012, **215**, 2869–2880.

[9] Chadwell B A, Standen E M, Lauder G V, Ashley-Ross M A. Median fin function during the escape response of bluegill sunfish (*Lepomis macrochirus*). II: Fin-ray curvature. *Journal of Experimental Biology*, 2012, **215**, 2881–2890.

[10] Tytell E D. Median fin function in bluegill sunfish Lepomis macrochirus: Streamwise vortex structure during steady swimming. *Journal of Experimental Biology*, 2006, **209**, 1516–1534.

[11] Maia A, Wilga C A. Function of dorsal fins in bamboo shark during steady swimming. *Zoology*, 2013, **116**, 224–231.

[12] Maia A, Lauder G V, Wilga C D. Hydrodynamic function of dorsal fins in spiny dogfish and bamboo sharks during steady swimming. *Journal of Experimental Biology*, 2017, **220**, 3967–3975

[13] Drucker E G, Lauder G V. Locomotor function of the dorsal fin in teleost fishes: Experimental analysis of wake forces in sunfish. *Journal of Experimental Biology*, 2001, **204**, 2943–2958.

[14] Drucker E G, Lauder G V. Wake dynamics and fluid forces of turning maneuvers in sunfish. *Journal of Experimental Biology*, 2001, **204**, 431–442.

[15] Hove J R, O'Bryan L M, Gordon M S, Webb P W, Weihs D. Boxfishes (Teleostei: Ostraciidae) as a model system for fishes swimming with many fins: Kinematics. *Journal of Experimental Biology*, 2001, **204**, 1459–1471.

[16] Borazjani I. The functional role of caudal and anal/dorsal fins during the C-start of a bluegill sunfish. *Journal of Experimental Biology*, 2013, **216**, 1658–1669.

[17] Standen E M, Lauder G V. Dorsal and anal fin function in bluegill sunfish Lepomis macrochirus: Three-dimensional kinematics during propulsion and maneuvering. *Journal of Experimental Biology*, 2005, **208**, 2753–2763.

[18] Tangorra J L, Lauder G V, Hunter I W, Mittal R, Madden P G, Bozkurttas M. The effect of fin ray flexural rigidity on the propulsive forces generated by a biorobotic fish pectoral fin. *Journal of Experimental Biology*, 2010, **213**, 4043–4054.

[19] Esposito C J, Tangorra J L, Flammang B E, Lauder G V. A robotic fish caudal fin: Effects of stiffness and motor program on locomotor performance. *Journal of Experimental Biology*, 2012, **215**, 56–67.

[20] Wen L, Wang T M, Wu G H, Linag J H,Wang C L. Novel method for the modeling and control investigation of efficient swimming for robotic fish. *IEEE Transactions on Industrial Electronics*, 2011, **59**, 3176–3188.

[21] Zhu J, White C, Wainwright D K, Di Santo V, Lauder G V, Bart-Smith H. Tuna robotics: A high-frequency experimental platform exploring the performance space of swimming fishes. *Science Robotics*, 2019, **4**, eaax4615.

[22] Conte J, Modarres-Sadeghi Y, Watts M N, Hover F S, Triantafyllou M S. A fast-starting mechanical fish that accelerates at 40 $m \cdot s^{-2}$. *Bioinspiration & Biomimetics*, 2010, **5**, 035004.

[23] Marchese A D, Onal C D, Rus D. Autonomous soft robotic fish capable of escape maneuvers using fluidic elastomer actuators. *Soft Robotics*, 2014, **1**, 75–87.

[24] Borazjani I. Simulations of unsteady aquatic locomotion: From unsteadiness in straight-line swimming to fast-starts. *Integrative and Comparative Biology*, 2015, **55**, 740–752.

[25] Bainbridge R. Speed and stamina in three fish. *Journal of Experimental Biology*, 1960, **37**, 129–153.

[26] Bandyopadhyay P R. Trends in biorobotic autonomous undersea vehicles. *IEEE Journal of Oceanic Engineering*, 2005, **30**, 109–139.

[27] Wu T Y. On theoretical modeling of aquatic and aerial animal locomotion. *Advances in Applied Mechanics*, 2002, **38**, 291–353.

[28] Witt W C, Wen L, Lauder G V. Hydrodynamics of C-start escape responses of fish as studied with simple physical models. *Integrative and Comparative Biology*, 2015, **55**, 728–739.

[29] Feilich K L, Lauder G V. Passive mechanical models of fish caudal fins: Effects of shape and stiffness on self-propulsion. *Bioinspiration & Biomimetic*, 2015, **10**, 036002.

[30] Akanyeti O, Thornycroft P J M, Lauder G V, Yanagitsuru Y R, Peterson A N, Liao J C. Fish optimize sensing and respiration during undulatory swimming. *Nature Communications*, 2016, **7**, 11044

[31] Eaton R C, Bombardieri R A, Meyer D L. The Mauthner-initiated startle response in teleost fish. *Journal of Experimental Biology*, 1977, **66**, 65–81.

[32] Tytell E D, Standen E M, Lauder G V. Escaping Flatland: Three-dimensional kinematics and hydrodynamics of median fins in fishes. *Journal of Experimental Biology*, 2008, **211**, 187–195.

[33] Frith H R, Blake R W. Mechanics of the startle response in the northern pike, Esox lucius. *Canadian Journal of Zoology*, 1991, **69**, 2831–2839.

[34] Webb P W. Effects of median-fin amputation on fast-start performance of rainbow trout (*Salmo gairdneri*). *Journal of Experimental Biology*, 1977, **68**, 123–135.

[35] Webb P W. Fast-start performance and body form in seven species of teleost fish. *Journal of Experimental Biology*, 1978, **74**, 211–216.